

## Comparing Twentieth- and Twenty-First-Century Patterns of Interannual Precipitation Variability over the Western United States and Northern Mexico\*

TYLER W. RUFF,<sup>+</sup> YOCHANAN KUSHNIR, AND RICHARD SEAGER

*Lamont-Doherty Earth Observatory, Columbia University, Palisades, New York*

(Manuscript received 12 October 2010, in final form 9 August 2011)

### ABSTRACT

The ability of coupled climate models to simulate the patterns of interannual precipitation variability over the western half of the United States and northern Mexico is investigated by applying principal component analysis to observations and model output. Global Precipitation Climatology Centre (GPCC) observations are compared to the pooled twentieth-century warm- and cold-season precipitation averages simulated by five coupled global climate models included in the Intergovernmental Panel on Climate Change Fourth Assessment Report. The pooled model spatial structures (EOFs) closely match those of the GPCC observations for both halves of the year. Additionally, the twenty-first-century model pooled EOFs are almost identical in spatial extent and amplitude to their twentieth-century counterparts. Thus, the spatial characteristics of large-scale precipitation variability in the western United States are not projected to change in the twenty-first century. When global observed and modeled seasonally averaged sea surface temperature anomalies are correlated with the time series corresponding to the three leading EOFs to discern sources of each mode of precipitation variability, a pattern reminiscent of El Niño is found to be the only significant association. The spatial structures of variability also appear independent of the model-predicted precipitation trend over the twenty-first century, indicating that the mechanisms responsible for the trend are different from those associated with interannual variability. The results of this study lend confidence in the pooled model predictions of seasonal precipitation patterns, and they suggest that future changes will primarily result from the contribution of the mean trend over which statistically stationary interannual variability is superimposed.

### 1. Introduction

The issue of a changing climatology of precipitation on regional scales under global warming has been examined, notably in the fourth Intergovernmental Panel on Climate Change (IPCC) assessment released in 2007. Averaging over 21 global climate models (GCMs) the Fourth Assessment Report (AR4) of the IPCC shows a trend of decreasing precipitation in the subtropics and increasing precipitation in most of the tropics and extratropics by the end of the twenty-first century (Solomon et al. 2007; Christensen et al. 2007). Concern over water resources in the American west, especially in the

Southwest, underlines the importance of accurate predictions of future trends in precipitation over this region. Studies (e.g., Seager et al. 2007; Cayan et al. 2010; Seager and Vecchi 2010) have shown that southwestern North America will experience a significant drying trend through the twenty-first century driven by increasing greenhouse gas concentrations. The same models also project an increase in the frequency of droughts of different time scales in the American west during the twenty-first century (Sheffield and Wood 2008). These projections led others to examine whether recent trends in various U.S. drought indicators can be detected and whether they are partly driven by anthropogenic forcing, with somewhat mixed results (e.g., Hidalgo et al. 2009; McCabe et al. 2010; Balling and Goodrich 2010). This is not surprising because short-term trends are strongly impacted by natural climate variability, particularly when the expected anthropogenic signal is rather weak.

Although predictions of mean precipitation change have been highly publicized, there has been less study regarding any change in the spatial and temporal structure

---

\* Lamont-Doherty Earth Observatory Publication Number 7495.

<sup>+</sup> Current affiliation: Commodity Weather Group, LLC, Bethesda, Maryland.

---

*Corresponding author address:* Yochanan Kushnir, Lamont-Doherty Earth Observatory, 61 Route 9W, Palisades, NY 10964.  
E-mail: kushnir@ldeo.columbia.edu

TABLE 1. The GCMs, chosen from the AR4 model suite in the Fourth Assessment Report of the IPCC, and observational datasets that were utilized in this paper. All model output is from their respective ensemble member referred to in the Program for Climate Model Diagnosis and Intercomparison (PCMDI) data portal as *run 1*.

IPCC designation	GCMs (country)	Observations
m04	GFDL CM2.0 (United States)	GPCC version 4
m05	GFDL CM2.1 (United States)	Second Hadley Centre SST dataset (HadSST2)
m14	Max Planck Institute (MPI) ECHAM5 (Germany)	
m16	NCAR CCSM3 (United States)	
m18	HadCM3 (United Kingdom)	

of variability of precipitation in the region. However, precipitation in the western United States and Mexico is highly variable in space and time. Accurate projections of the future require models to be able to represent this variability and how it may change over time.

In this paper we study the observed patterns of variability over the western United States and address the ability of the IPCC AR4 models to simulate these patterns. We also compare the model simulations of these patterns in the twenty-first century with their twentieth-century counterparts. Because El Niño–Southern Oscillation (ENSO) forces a coherent, large-scale pattern of interannual precipitation variability, particularly within the Pacific basin and over the surrounding continents, it is expected to produce the strongest signal in the study area during both centuries. This link is explored in both observations and models and for the winter and summer half years separately. We do not focus on the differences between the models themselves but, instead, provide a synopsis on the strengths of the models as a composited group.

## 2. Data and methods

We use the Global Precipitation Climatology Centre (GPCC) version 4 precipitation dataset with 2.5° horizontal resolution (Schneider et al. 2008) to compare against five global climate models featured in the 2007 IPCC report. An overview of the methods employed to ensure a high quality standard for the GPCC dataset can be found in Schneider et al. (2008) and Beck et al. (2005). This resolution is sufficient to capture the subcontinental details that are resolvable by the models, all of which were run at or near 2.5° resolution and interpolated to match the grid of the observations. Because we do not aim to produce an exhaustive model study but rather to test the hypothesis that the models provide a reasonable simulation of the observed behavior, we limit the model selection to five models that are widely used and well documented: the Geophysical Fluid Dynamics Laboratory Climate Model version 2.0 (GFDL CM2.0), GFDL CM2.1, ECHAM5, National Center for Atmospheric Research Community Climate System Model version

3 (NCAR CCSM3), and third climate configuration of the Met Office Unified Model (HadCM3). For reference, all datasets used in this study are listed in Table 1. For the simulation with these models we use the datasets created by the Coupled Model Intercomparison Project 3 (CMIP3). The twentieth-century (here 1901–99) simulations were forced with known or estimated changes in atmospheric trace gases, solar irradiance, and volcanism. The twenty-first-century (2001–99) projections were taken from the output of the same models' integrations as provided in the IPCC AR4 archive (<https://esg.llnl.gov:8443/index.jsp>). These model integrations were forced with the so-called “middle of the road” A1B emissions scenario (see Nakicenovic and Swart 2000) starting from initial conditions taken from the last year of output of the CMIP3 runs (for detailed description of the models and the output, see [http://www-pcmdi.llnl.gov/ipcc/model\\_documentation/ipcc\\_model\\_documentation.php](http://www-pcmdi.llnl.gov/ipcc/model_documentation/ipcc_model_documentation.php)). Only one realization per century was picked for each of the participating models so as not to bias the results to any particular one.

Principal component analysis (PCA) is used to determine the primary modes of variability in precipitation on a subcontinental scale. The PCA method separates the space–time variability into the spatial structures (eigenvectors of the covariance matrix of the data) and their corresponding time-dependent coefficients, such that the residual variance over the domain of analysis is progressively minimized. The resulting structures and time series are then arranged by order of the fraction of total variance explained and thus allow the extraction of the leading patterns of variability in the data (e.g., Wilks 2006). The PCA is applied to spatially weighted data (i.e., we take into account the changes in the area represented by each grid box with changing latitude). The structures presented in the figures are shown without the area weighting and multiplied by the corresponding eigenvalue, such that the field values are in units of percentage of climatology. Note that in this paper the “climatology” of a field is the mean of a season taken over an entire century.

The overlapping time interval between the observations and the twentieth-century model simulations is from

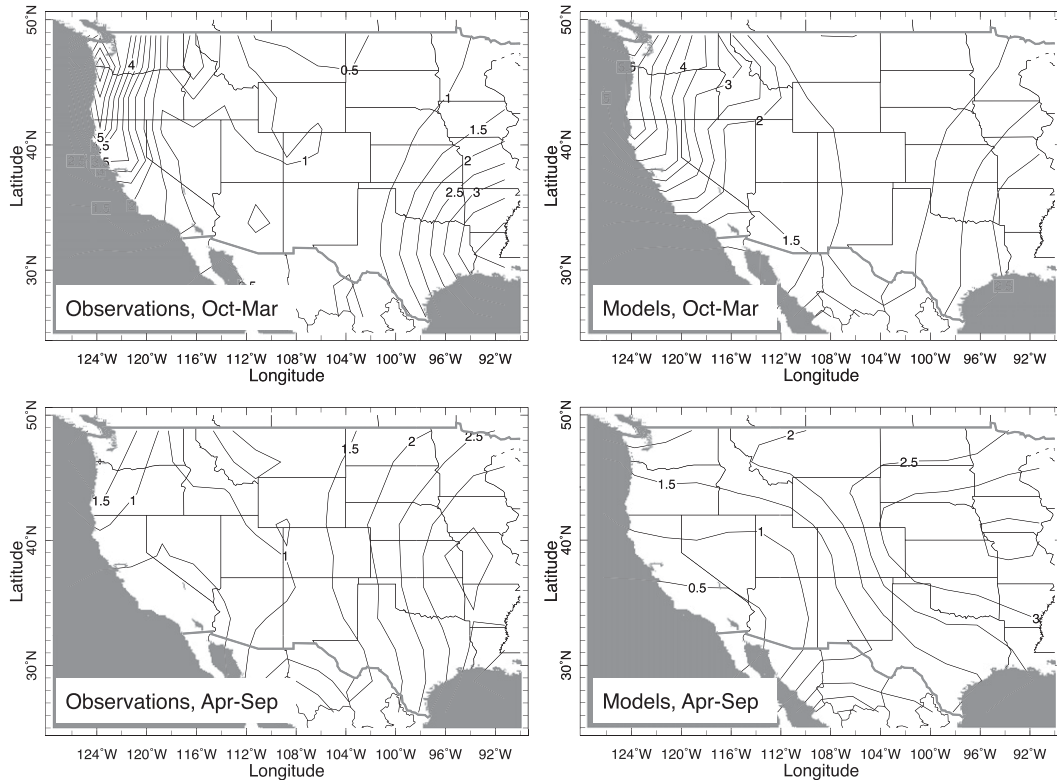


FIG. 1. Climatology of (left) the GPCC precipitation observations and (right) the five-model average precipitation over the western United States for the twentieth century for (top) the October–March and (bottom) April–September periods (bottom). Contours are shown every  $0.5 \text{ mm day}^{-1}$ .

1901 through 1999. The precipitation anomalies were analyzed over the months of October–March and April–September for each year, corresponding to the first and second halves of the “hydrologic year” (also referred to as “water year”; see definition in the American Meteorological Society’s *Glossary of Meteorology*, which can be found online at <http://amsglossary.allenpress.com/glossary>). These are referred to as the “winter” and the “summer” seasons, respectively. Because our interest is in the variability of precipitation in the western United States, we focus on the contiguous United States west of the Ohio–Mississippi Valley (west of longitude  $90^\circ\text{W}$ ). To account for model biases in simulating the climatology of precipitation (see section 3), the precipitation anomalies derived from observations and model output were normalized by their respective 1901–99 climatologies:

$$P'(x, y, t) = \frac{P(x, y, t) - P_c(x, y)}{P_{c20}(x, y)},$$

where  $P(x, y, t)$  denotes the seasonal total precipitation for year  $t$  at longitude  $x$  and latitude  $y$ , the subscript  $c$  indicates the climatology of the relevant season and century, and  $c20$  indicates the twentieth-century

climatological value. That is, each gridpoint value in the seasonal anomaly fields was divided by the seasonal twentieth-century climatological value at that point before applying the PCA. Thus the patterns shown represent patterns of seasonal variability as a fraction of the corresponding seasonal twentieth-century climatology. This approach was taken primarily in order to account for model spatial and intensity biases, representing models and observations in a more compatible metric. We define the twenty-first century as the time period from 2001 through 2099, and the model runs for this time period were generated as in the twentieth-century runs except forced by a moderate greenhouse emissions scenario.

A procedure often applied to PCA results, referred to as PCA “rotation” (RPCA; Wilks 2006), was also attempted in this study. RPCA relaxes the constraint of variance maximization and spatial orthogonality to produce more localized maxima and minima. To assess which of the two methods, PCA or RPCA, lends itself to more direct physical interpretation, we correlated the resulting time series with global sea surface temperatures (SSTs) and sea level pressure. We found that none of the leading rotated structure yields any coherent connections, particularly not the expected correlation to

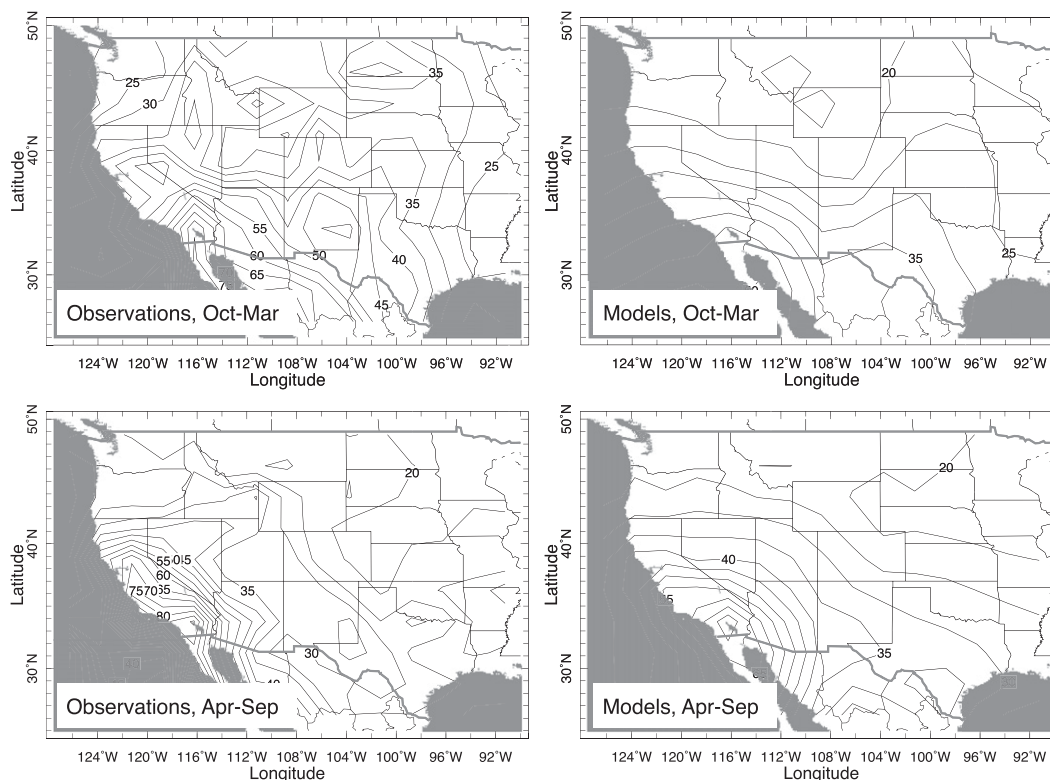


FIG. 2. Root-mean-square values of seasonal precipitation variability divided locally by the climatological precipitation expressed in percent: (left) observations and (right) the models. Contours are shown every 5%.

Pacific or Atlantic SSTs (see, e.g., Kushnir et al. 2010 and references therein). Of the nonrotated time series, however, the leading pattern did reveal a clear link to El Niño (see section 5). We therefore concluded that the results of the nonrotated analysis make more physical sense than the rotated one and chose to present and compare the nonrotated structures.

While we did examine the variability in each model separately, the presentation here will focus on the features common to all five models as represented by the multimodel ensemble. Adopting such a “common EOF” approach (e.g., Barnett 1999) to the analysis of model output reflects the general perception that multimodel ensembles compensate for each model’s particular bias to produce a more “realistic” representation of nature. While this assumption is based on empirical evidence, the multimodel approach has been adopted by numerous studies of detection and attribution of climate variability and change (see Meehl et al. 2007 and references therein).

In the present adoption of the common EOF analysis, all model anomalies were placed on the same spatial grid strung one after the other in the time domain to calculate a common covariance matrix, which is equivalent to the average of all individual model covariance matrices.

The diagonalization of this common covariance matrix leads to spatial patterns (EOFs) for which the time coefficients (PCs) can be broken up by model to give the information on how the corresponding structure changes in time for each model separately. For root-mean-square (RMS) variability we present the square root of the variance averaged over all five models (this is equivalent to calculating the variance of the pooled model anomalies). Where individual models behave notably different from the multimodel ensemble mean, we mention this in the text. The pooled multimodel fields were appreciably smoother than the single-sample observed field; therefore, to facilitate easier comparison between them and the observed field analysis, a single pass of a two-dimensional binomial smoother (a 1–2–1 weighted average of each grid point with its closest two grid points in latitude and longitude) was applied to the latter.

### 3. Seasonal climatology and variability

The multimodel mean and GPCP observations of the seasonal climatology of precipitation over the western United States for the twentieth century is displayed in Fig. 1 for the winter and summer halves of the year. The corresponding RMS values for the same fields are



TABLE 2. The first three normalized eigenvalues (EV) of the model and observation precipitation field EOFs over the western United States. Note that these are calculated after normalization by the respective climatology of each dataset for the century and season of interest.

Model normalized eigenvalues					
	EV	Twentieth century		Twenty-first century	
		Winter	Summer	Winter	Summer
m04	1	0.35	0.28	0.36	0.34
	2	0.21	0.14	0.16	0.14
	3	0.08	0.13	0.09	0.11
m05	1	0.37	0.24	0.32	0.23
	2	0.18	0.16	0.17	0.18
	3	0.08	0.10	0.09	0.10
m14	1	0.25	0.30	0.27	0.25
	2	0.20	0.13	0.16	0.18
	3	0.12	0.13	0.10	0.12
m16	1	0.23	0.20	0.27	0.21
	2	0.2	0.16	0.23	0.15
	3	0.15	0.09	0.12	0.10
m18	1	0.48	0.37	0.41	0.32
	2	0.12	0.17	0.15	0.15
	3	0.08	0.08	0.08	0.12
Pooled	1	0.34	0.24	0.33	0.25
	2	0.18	0.17	0.18	0.17
	3	0.12	0.12	0.10	0.12

Observation normalized EVs			
	EV	Twentieth century	
		Winter	Summer
GPCC	1	0.37	0.24
	2	0.14	0.16
	3	0.10	0.09

the twentieth century are 0.92, 0.93, and 0.84, respectively (Table 3, top). EOF orthogonality constraints may be partially responsible for the commonality between higher-order patterns once the leading patterns are similar. However, this overall agreement confirms the ability of the models to correctly represent the broad features of the primary structures of precipitation variability during the winter season.

The right column in Fig. 3 displays the same results but for the twenty-first-century model projections. The patterns appear almost identical to those for the twentieth century. As we will show later, the first eigenvector is characteristic of the precipitation variability arising from the remote influence of tropical Pacific SSTs. Four of the five models produced reasonably similar patterns, with one exception being the NCAR CCSM3, which displays a nodal line through the middle latitudes of the United States instead of curving north of the Great Plains as in the other models (not shown). This may be expected because of the poor ENSO simulation by the NCAR model (Deser et al. 2006), which has been shown to be a result of its weaker simulated large-scale atmospheric

TABLE 3. Spatial correlations between the pooled model composite and GPCC observations of EOFs of western U.S. precipitation patterns for (top) both seasons for the twentieth century and (bottom) between the model precipitation fields for the twentieth and twenty-first centuries.

Pooled model and observation correlations for the twentieth century			
EV	Winter	Summer	
1	0.92	0.66	
2	0.93	0.71	
3	0.84	0.22	

Model correlations between the twentieth and twenty-first centuries			
EV	Winter	Summer	
1	0.99	0.93	
2	0.97	0.95	
3	0.95	0.97	

response to tropical Pacific SST anomalies in comparison to other models (Capotondi and Alexander 2010).

The corresponding results for the summer period (April–September) are displayed in Fig. 4. The first three eigenvectors of the GPCC data (left column) represent 24%, 16%, and 9% (total 49%) of the total variance in the dataset, respectively. The model average eigenvectors for the same period (center column) account for 24%, 17%, and 12% (total 53%), respectively, of the total variance for the dataset (Table 2). Spatial correlation values between the first three eigenvectors of the model composite and the observations are 0.66, 0.71, 0.22, respectively (Table 3, top), indicating a weaker agreement than in the winter season, especially in the third eigenvector. The spatial correlation values between the eigenvectors of the model composites for the two centuries are very close to 1 in both seasons (Table 3, bottom). The differences between the models and the observations in how the total variance is distributed amongst the first three eigenvectors may not be significant, but the models, relative to observations, place more variance in the second and third eigenvectors than in the first. In both datasets, there is about 12% less total variance contained within the first three eigenvectors in the summer than in the winter. We suspect that this is a result of the weaker control exerted by the large-scale ocean–atmosphere conditions over precipitation variability in summer compared to winter (e.g., Seager et al. 2009; Kushnir et al. 2010) and of the more local, and less organized nature of the convective summer precipitation.

Figure 5 displays the normalized eigenvalues for the first five eigenvectors of the observations and combined-model EOFs for the twentieth and twenty-first century and for the cold and warm seasons. The figure shows a good agreement between the observations and models

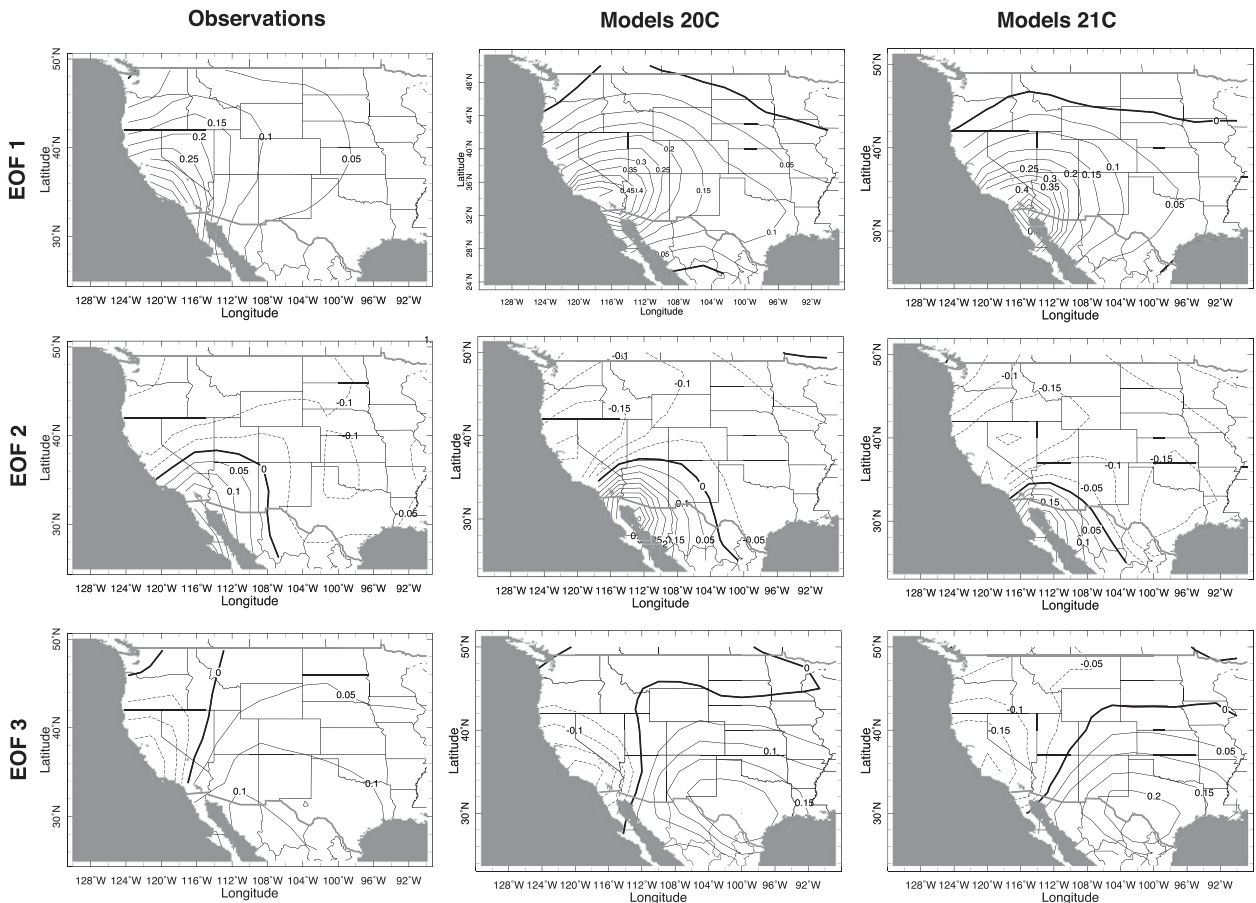


FIG. 4. As in Fig. 3, except for the period of April–September.

and between the twentieth and twenty-first century, indicating that the models accurately simulate the precipitation variability (as percentage of the twentieth-century climatology) and that the structure of variability is not projected to change in the future.

### 5. Global sea surface temperature correlations

To discern the source of variability underlying the structures present in the principal components in the twentieth century, the time series of the leading eigenvectors of the observations were correlated with global SST by season. For the observations, the Met Office Hadley Centre Sea Ice and Sea Surface Temperature (HadISST) dataset (Rayner et al. 2003) was used. Here, only the correlation patterns corresponding to the first EOF is discussed, as it is the only one that exhibits a clear, known, and significant pattern.

The correlation pattern between the time series corresponding to EOF1 (hereafter PC1) derived from observations and from the pooled model output are shown

in the top panels of Figs. 6 and 7 for the cold (October–March) and warm (April–September) seasons, respectively (note that because this is a linear analysis, the opposite-signed patterns are equally as valid). Also shown in these figures (in the lower panels) are the corresponding correlations between the Niño-3.4 index (calculated by averaging the anomalous SST values between 5°S–5°N and 170°–120°W) and the SST field. The resemblance between the PC1 correlations and those of Niño-3.4 is striking; though, as expected, the strength of the correlations is weaker when PC1 is used (note that based on a parametric inference test and assuming that annual values are independent, correlation values greater than 0.2 or less than  $-0.2$  are significant at the 95% level).

In observations (Figs. 6a and 7a for PC1 correlations and Figs. 6c and 7c for Niño-3.4 correlations), the typical cold- and warm-season El Niño patterns display a broad warm SST anomaly in the eastern tropical Pacific straddled by cold anomalies in the sub- and extratropics with warm anomalies in the Indian Ocean and along the

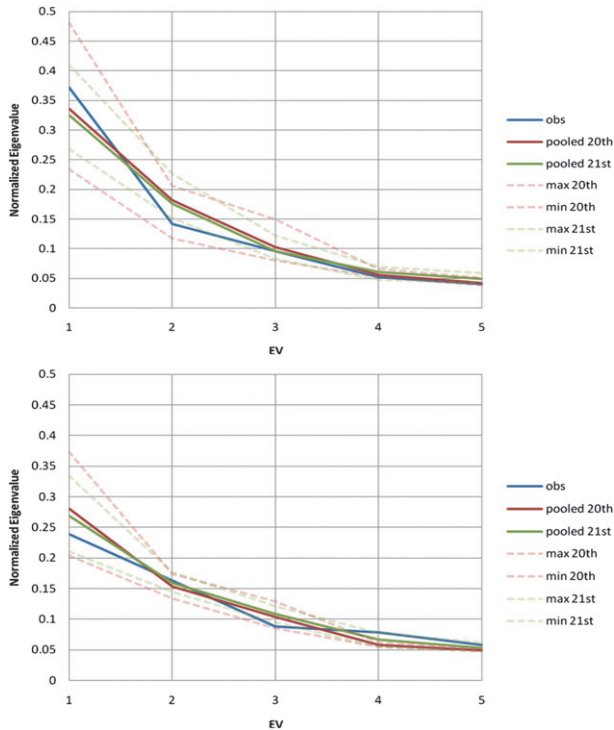


FIG. 5. Normalized eigenvalue curves for the first five leading observed and combined-model EOFs for the twentieth and twenty-first centuries for (top) the cold season (October–March) and (bottom) the warm season (April–September). The dashed lines represent the highest and lowest value from among the individual models for each EOF.

western North American seaboard. According to Fig. 3 and Figs. 6 and 7, this situation thus corresponds to a wetter-than-normal southwest United States and northern Mexico.

A similar correlation analysis was applied to the model output, stringing together in time the five-model global SST anomaly fields and correlating the pooled data with the pooled PC time series. Again, only the first pattern exhibited a significant relationship to the cold- and warm-season SST fields, which corresponded well to the observations (Figs. 6b and 7b) and closely resemble the corresponding correlations between the models' pooled Niño-3.4 index and the pooled SST field (Figs. 6d and 7d). These results confirm that the models correctly implicate tropical Pacific SST variability as a playing a distinctive external control on precipitation variability over the western United States, especially in the winter season.

Further evidence to the link between tropical Pacific SST variability and the pattern of precipitation variability captured by the leading EOF is provided in Fig. 8, where the times series of PC1 and the corresponding Niño-3.4 indices for observations and each model separately are shown together with the corresponding correlation values.

The time series also show that the variability is dominated by relatively high-frequency year-to-year fluctuations (i.e., the variability associated with ENSO).

It is important to note that four of the models, when tested individually, produce fairly similar results. The exception is the NCAR model, which has a rather weak link between tropical Pacific SST anomalies and precipitation over North America (as described earlier). This may explain the somewhat lower (in the absolute sense) values found in the multimodel correlation fields. The temporal correlations were also repeated with model and observational global sea level pressure fields, again revealing a strong ENSO-related pattern for the leading PC and no clear signal in the others (not shown).

The corresponding model twenty-first-century PC1 correlation fields are shown in Fig. 9 (top panel) for the cold season only. The SST correlations for the twenty-first century closely resemble those for the twentieth century in spatial extent but the strength of the positive (tropical) and negative (extratropical) regions is reduced compared to the former. Bearing in mind that the models also predict a significant worldwide SST warming trend during the twenty-first century, we repeated the calculation, removing the SST linear trend. The results (Fig. 9, bottom panel) show larger correlation values that match the twentieth-century values much closer but are still slightly weaker.

## 6. The precipitation trend

The PCA method accurately reveals the unique role of ENSO in forcing western United States precipitation variance, particularly during winter. According to the models, the spatial pattern of ENSO-forced variability remains essentially the same in the twenty-first century as in the twentieth century. However, it is possible that the trend in precipitation is influenced by changes in the frequency and intensity of ENSO events in the twenty-first century. To this we add the fact that precipitation anomalies may increase in amplitude because of the increase in atmospheric-specific humidity associated with warming (Held and Soden 2006; Seager and Vecchi 2010). Separating the dynamical impact (changes in ENSO) from the thermodynamic one is beyond the scope of this paper. Here we resort to a brief examination of the linear trend in western U.S. precipitation.

The five-model composite twenty-first-century linear trend in precipitation, relative to climatology, over the western United States, by season, is shown in Fig. 10. In this calculation, consistent with the methodology used in the PCA, each model's seasonal precipitation anomaly was first normalized by its twentieth-century seasonal climatology before averaging over all models. In the cold

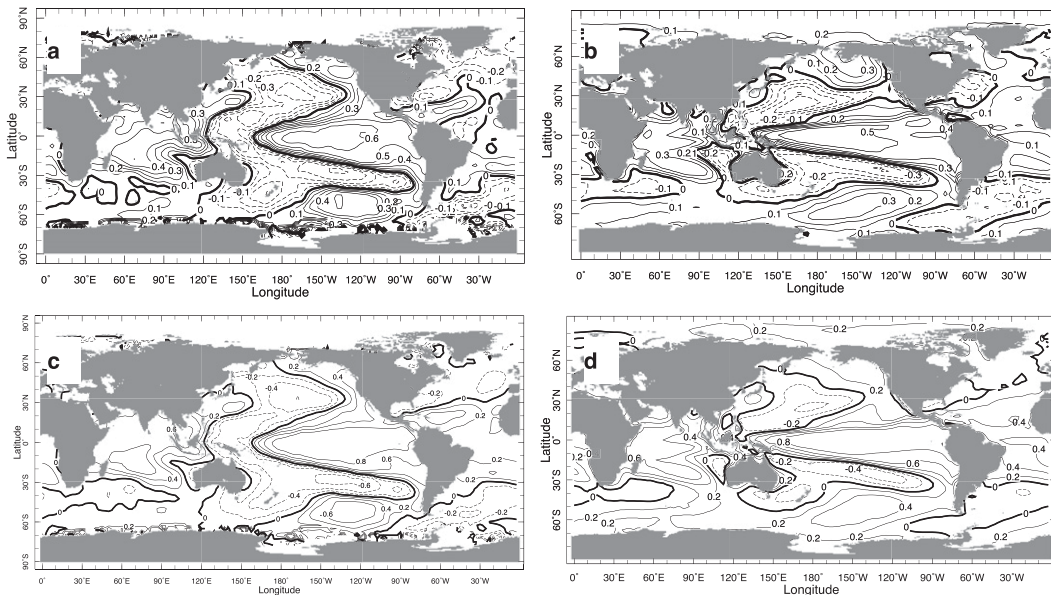


FIG. 6. (a) Correlation between the first EOF of observed western U.S. precipitation with observed global SST field for the twentieth century and for the cold season (October–March average), and (b) the same, but for the common model EOF and the pooled model simulated SST fields. (c) Correlation between the observed Niño-3.4 index and observed global SST field for the twentieth century during the cold season, and (d) the same, but for the pooled model Niño-3.4 index and the pooled model global SST field. The contour interval in (a),(b) is 0.1 and in (c),(d) is 0.2.

season, a clear drying trend is confined to the west coast, from California through northern Mexico, while a wetting trend is prevalent through the rest of the United States. In the summer, the drying trend is more widespread, reaching all the states bordering the Pacific Ocean and the Gulf of Mexico, while a wetting trend is weaker

and concentrated to the Midwest. This is consistent with the results of the entire AR4 model suite of the 2007 IPCC report (Christensen et al. 2007, their Fig. 11.12). Figure 10 also shows (by different shades of gray) the number of models (out of the five total in the composite) that agree on the sign of the trend in the respective grid

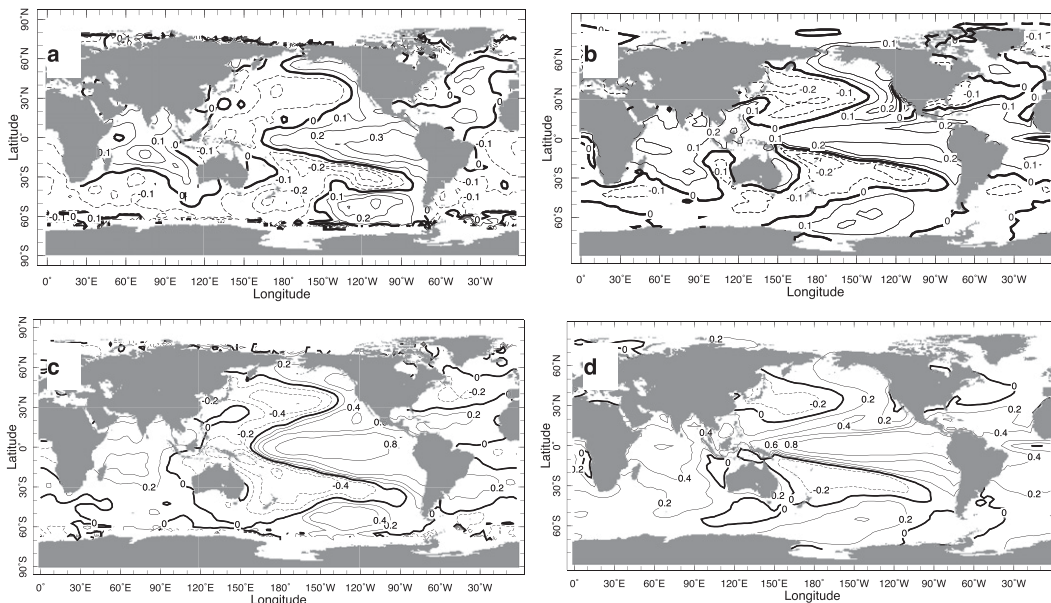


FIG. 7. As in Fig. 6, but for the warm season (April–September average).

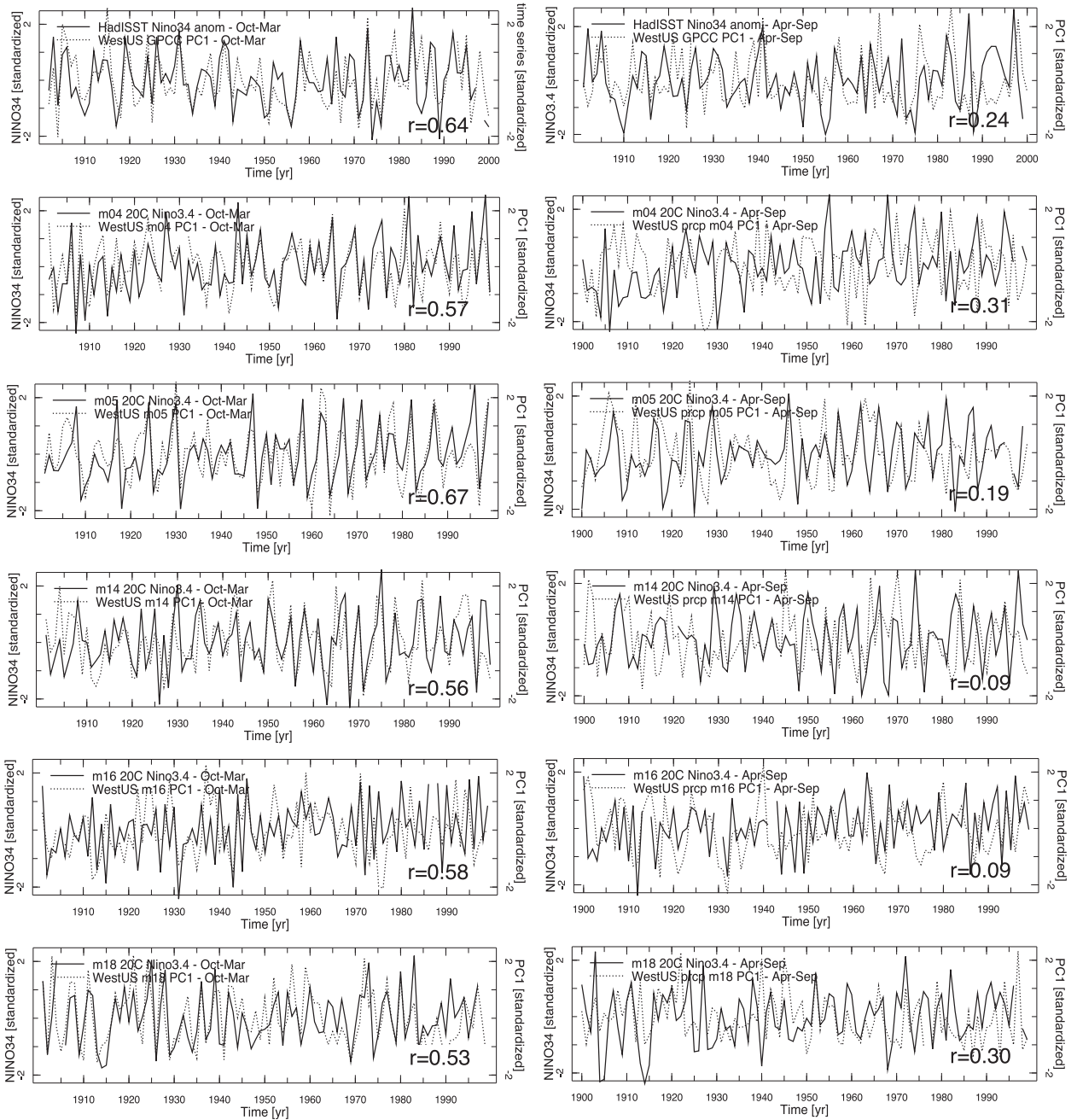


FIG. 8. Time series of western U.S. precipitation PC1 calculated from (top) observations and (second row to bottom row) the pooled model output, shown together with the corresponding observed and modeled Niño-3.4 index, respectively, for the (left) cold and (right) warm seasons. All time series are normalized to have unit variance over the years shown. Also displayed are the linear correlations between each two time series.

box. In the winter season, at least four models generally agree over areas that show a roughly  $\pm 10\%$  trend in the composite, while in the summer the agreement is less extensive but is still strong in the south and west United States and northern Mexico. The predominant agreement among individual models lends confidence in our

decision to use the model composite (Fig. 10) for the discussion of the twenty-first-century trend.

As shown in Seager and Vecchi (2010) and Seager et al. (2010), because of warming, the region of decline in precipitation minus evaporation—the net flux of water substance at the surface—extends farther north than the

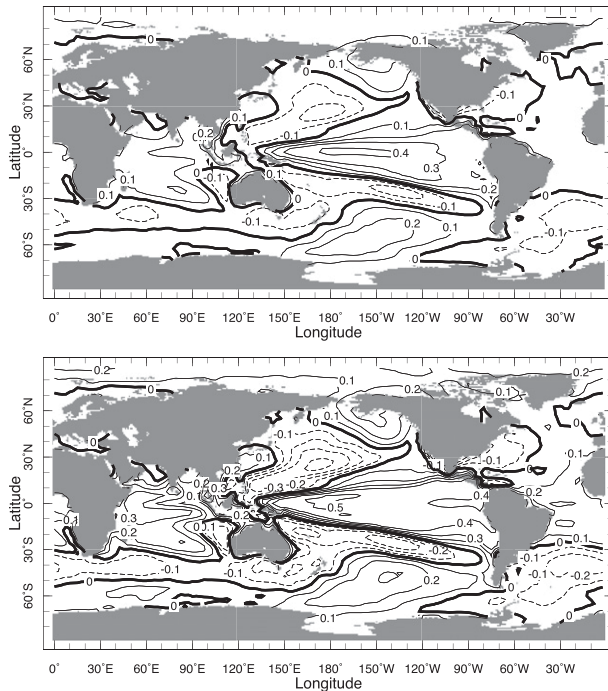


FIG. 9. (top) The correlation between the leading combined PC of modeled, twenty-first century, western U.S. precipitation and the corresponding simulated global SST field for October–March. (bottom) As above but for linearly detrended SST.

region of precipitation decrease and encompasses a wider swath of southwestern North America (also note that here we analyze only 5 models compared to the 15 analyzed by Seager and Vecchi 2010 and Seager et al. 2010). Seager and Vecchi (2010) (see also Seager et al. 2010) have shown that the drying across the subtropics and over southwestern North America is caused by 1) increased divergence of moisture by the mean divergent flow, which is a consequence of rising humidity in warming air; and 2) reduced convergence of moisture by transient eddies. In addition, a poleward extension of the Hadley cell and poleward shift of the storm tracks causes the subtropical dry zones to expand poleward. The trend pattern in Fig. 10 is not clearly related to any single EOF pattern in Figs. 3 and 4, supporting the assertion that the mechanisms responsible for it are different than those associated with interannual variability.

## 7. Summary and conclusions

The principal component analysis of precipitation over southwestern North America generated for our five-IPCC-model composite produces results that are very similar in spatial extent and amplitude to those of the GPCP observations for both the winter (October–March) and summer (April–September) halves of the year. When

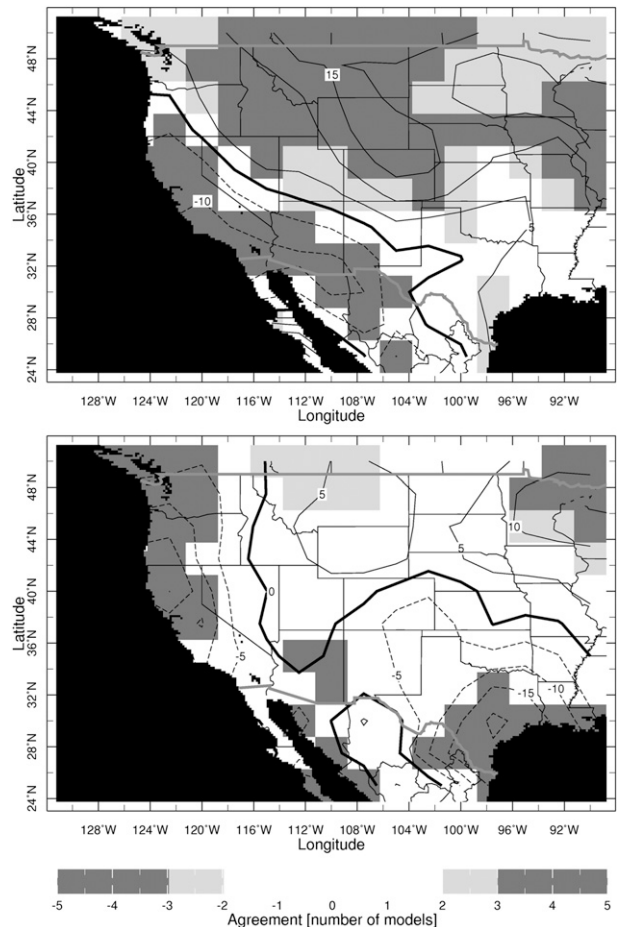


FIG. 10. The trend in precipitation of the twenty-first century averaged for the five IPCC global climate models during (top) October–March and (bottom) April–September. The units are change over 100 yr as percent of the twentieth-century climatology of the respective model. The figures are overlaid with shading corresponding to the number of models (out of five) that agreed on the sign of the trend over each grid box. Dark gray indicates agreement among four or five models, light gray for three models, and white for fewer than three models.

combined, the first three eigenvectors for the models account for more than half the total variance in their respective datasets for both seasons and both centuries. Likewise, the model composite EOFs for twenty-first-century winters and summers are almost identical in spatial extent and amplitude to the twentieth-century ones. Four of the five models reduce the contribution of the sum of the first three normalized eigenvalues in the twenty-first century compared to the twentieth century. The model SST correlations with the PCA time series of western United States precipitation show a strong ENSO pattern in the first eigenvector with a weaker amplitude in the twenty-first century, while the next two eigenvectors do not show a strong recognizable

associated signal in SST (or sea level pressure); this suggests that their pattern is related to the PCA orthogonality constraint. Throughout the study, the NCAR CCSM3 is the only model that deviates significantly from the other models and the observations in all of the above analyses, which is likely because of its relatively poor simulation of ENSO.

As we showed, the model composite produces a reliable simulation of the spatial pattern of ENSO-forced precipitation variability. Barring the possibility that this is due to compensating errors that might not balance so well in the future state of the climate, projections made by these models can be trusted with some confidence. If so, then the results shown here suggest that anthropogenic forcing will not significantly alter the spatial pattern of the primary mode of interannual precipitation variability across North America. In these five models the spatial patterns of variability do not appreciably change; the distribution of variance among the patterns of variability changes little, as does the role of the external influence of tropical Pacific SST variability. Whether ENSO characteristics are affected (or not) by global warming is an unresolved subject (see Vecchi and Wittenberg 2010). The models we examined do not seem to indicate such changes. These same models, like almost all models used as part of AR4, simulate a downward secular trend in winter precipitation over southwestern North America (Seager et al. 2007). According to the model projections, interannual variability around this drying trend will occur with essentially the same amplitude and spatial pattern as is familiar from the twentieth century. It will be interesting to test these conclusions using more climate models including the simulations and projections now being done as part of CMIP5.

*Acknowledgments* We would like to acknowledge help from Naomi Naik and Jennifer Nakamura in data preparation, computation, and other technical issues. This study was supported by NOAA Grant NA08OAR4320912 to the Cooperative Institute of Climate Applications and Research and NSF Grant ATM-08-04107. T. Ruff also acknowledges the support of the LDEO Summer Intern Programs for Undergraduates.

#### REFERENCES

- Balling, R., and G. Goodrich, 2010: Increasing drought in the American Southwest? A continental perspective using a spatial analytical evaluation of recent trends. *Phys. Geogr.*, **31**, 293–306, doi:10.2747/0272-3646.31.4.293.
- Barnett, T. P., 1999: Comparison of near-surface air temperature variability in 11 coupled global climate models. *J. Climate*, **12**, 511–518.
- Beck, C., J. Grieser, and B. Rudolf, 2005: A new monthly precipitation climatology for the global land areas for the period 1951 to 2000. Klimastatusbericht KSB 2004, 181–190. [Available online at <http://gpcc.dwd.de/>.]
- Capotondi, A., and M. A. Alexander, 2010: Relationship between precipitation in the Great Plains of the United States and global SSTs: Insights from the IPCC AR4 models. *J. Climate*, **23**, 2941–2958.
- Cayan, D. R., T. Das, D. W. Pierce, T. P. Barnett, M. Tyree, and A. Gershunov, 2010: Future dryness in the southwest US and the hydrology of the early twenty-first century drought. *Proc. Natl. Acad. Sci. USA*, **107**, 21 271–21 276.
- Christensen, J. H., and Coauthors, 2007: Regional climate projections. *Climate Change 2007: The Physical Science Basis*, S. Solomon et al., Eds., Cambridge University Press, 847–940.
- Deser, C., A. Capotondi, R. Saravanan, and A. S. Phillips, 2006: Tropical Pacific and Atlantic climate variability in CCSM3. *J. Climate*, **19**, 2451–2481.
- Held, I. M., and B. J. Soden, 2006: Robust responses of the hydrological cycle to global warming. *J. Climate*, **19**, 5686–5699.
- Hidalgo, H. G., and Coauthors, 2009: Detection and attribution of streamflow timing changes to climate change in the western United States. *J. Climate*, **22**, 3838–3855.
- Kushnir, Y., R. Seager, M. Ting, N. Naik, and J. Nakamura, 2010: Mechanisms of tropical Atlantic SST influence on North American precipitation variability. *J. Climate*, **23**, 5610–5628.
- McCabe, G. J., D. R. Legates, and H. F. Lins, 2010: Variability and trends in dry day frequency and dry event length in the southwestern United States. *J. Geophys. Res.*, **115**, D07108, doi:10.1029/2009JD012866.
- Meehl, G. A., C. Covey, T. Delworth, M. Latif, B. McAvaney, J. F. B. Mitchell, R. J. Stouffer, and K. E. Taylor, 2007: The WCRP CMIP3 multimodel dataset: A new era in climate change research. *Bull. Amer. Meteor. Soc.*, **88**, 1383–1394.
- Nakicenovic, N., and R. Swart, Eds., 2000: *Emissions Scenarios*. Cambridge University Press, 599 pp.
- North, G. R., T. L. Bell, R. F. Cahalan, and F. J. Moeng, 1982: Sampling errors in the estimation of empirical orthogonal functions. *Mon. Wea. Rev.*, **110**, 699–706.
- Rayner, N. A., D. E. Parker, E. B. Horton, C. K. Folland, L. V. Alexander, D. P. Rowell, E. C. Kent, and A. Kaplan, 2003: Global analyses of sea surface temperature, sea ice, and night marine air temperature since the late nineteenth century. *J. Geophys. Res.*, **108**, 4407, doi:10.1029/2002JD002670.
- Schneider, U., T. Fuchs, A. Meyer-Christoffer, and B. Rudolf, 2008: Global precipitation analysis products of the GPCC. Global Precipitation Climatology Centre and DWD Tech. Rep., 12 pp. [Available online at [ftp://ftp.dwd.de/pub/data/gpcc/PDF/GPCC\\_intro\\_products\\_2008.pdf](ftp://ftp.dwd.de/pub/data/gpcc/PDF/GPCC_intro_products_2008.pdf).]
- Seager, R., and G. A. Vecchi, 2010: Greenhouse warming and the 21st century hydroclimate of southwestern North America. *Proc. Natl. Acad. Sci. USA*, **107**, 21 277–21 282.
- , and Coauthors, 2007: Model projections of an imminent transition to a more arid climate in southwestern North America. *Science*, **316**, 1181–1184.
- , and Coauthors, 2009: Mexican drought: An observational modeling and tree ring study of variability and climate change. *Atmósfera*, **22**, 1–31.
- , N. Naik, and G. A. Vecchi, 2010: Thermodynamic and dynamic mechanisms for large-scale changes in the hydrological

- cycle in response to global warming. *J. Climate*, **23**, 4651–4668.
- Sheffield, J., and E. F. Wood, 2008: Projected changes in drought occurrence under future global warming from multi-model, multi-scenario, IPCC AR4 simulations. *Climate Dyn.*, **31**, 79–105.
- Solomon, S., D. Qin, M. Manning, M. Marquis, K. Averyt, M. M. B. Tignor, H. L. Miller Jr., and Z. Chen, Eds., 2007: *Climate Change 2007: The Physical Science Basis*. Cambridge University Press, 996 pp.
- Vecchi, G. A., and A. T. Wittenberg, 2010: El Niño and our future climate: Where do we stand? *Wiley Interdiscip. Rev.: Climate Change*, **1**, 260–270, doi:10.1002/wcc.33.
- Wilks, D. S., 2006: *Statistical Methods in the Atmospheric Sciences*. 2nd ed. International Geophysics Series, Vol. 59, Academic Press, 627 pp.